Boundary-Layer Meteorol (2007) 122:493–515
DOI 10.1007/s10546-006-9117-x

ORIGINAL PAPER

The ejection-sweep cycle over bare and forested gentle hills: a laboratory experiment

D. Poggi · G. Katul

Received: 6 December 2005 / Accepted: 24 July 2006 /
Published online: 11 November 2006

Abstract Progress on practical problems such as quantifying gene flow and seed dispersal by wind or turbulent fluxes over nonflat terrain now demands fundamental understanding of how topography modulates the basic properties of turbulence. In particular, the modulation by hilly terrain of the ejection-sweep cycle, which is the main coherent motion responsible for much of the turbulent transport, remains a problem that has received surprisingly little theoretical and experimental attention. Here, we investigate how boundary conditions, including canopy and gentle topography, alter the properties of the ejection-sweep cycle and whether it is possible to quantify their combined impact using simplified models. Towards this goal, we conducted two new flume experiments that explore the higher-order turbulence statistics above a train of gentle hills. The first set of experiments was conducted over a bare surface while the second set of experiments was conducted over a modelled vegetated surface composed of densely arrayed rods. Using these data, the connections between the ejection-sweep cycle and the higher-order turbulence statistics across various positions above the hill surface were investigated. We showed that ejections dominate momentum transfer for both surface covers at the top of the inner layer. However, within the canopy and near the canopy top, sweeps dominate momentum transfer irrespective of the longitudinal position; ejections remain the dominant momentum transfer mode in the whole inner region over the bare surface. These findings were well reproduced using an incomplete cumulant expansion and the measured profiles of the second moments of the flow. This result was possible because the variability in the flux-transport terms, needed in the incomplete cumulant expansion, was shown to be well modelled using "local" gradient-diffusion principles. This result suggests that, in the inner layer, the higher-order turbulence statistics appear to be much more impacted by their relaxation history towards equilibrium rather

D. Poggi
Dipartimento di Idraulica, Trasporti ed Infrastrutture Civili Politecnico di Torino, Torino, Italy

G. Katul (✉)
Nicholas School of the Environment and Earth Sciences, Duke University, Durham, NC, USA
e-mail: gaby@duke.edu

than the advection-distortion history from the mean flow. Hence, we showed that it is possible to explore how various boundary conditions, including canopy and topography, alter the properties of the ejection-sweep cycle by quantifying their impact on the gradients of the second moments only. Implications for modelling turbulence using Reynolds-averaged Navier Stokes equations and plausible definitions for the canopy sublayer depth are briefly discussed.

Keywords Canopy turbulence · Closure models · Cumulant expansion · Ejections and sweeps · Flow over gentle hills · Nonlocal transport

1 Introduction

Understanding the modulation of organized motion by complex terrain near boundaries, bare or vegetated, remains a central research topic- now stimulated by a diverse set of applications. These applications include numerical models for wind engineering and urban pollution that employ Reynolds-averaged Navier–Stokes equations (RANS) (e.g. see the recent review in Bitsuamlak et al. 2004), the proliferating number of studies on CO_2 scalar fluxes near the land surface in complex terrain (e.g. Baldocchi et al. 2000, 2001; Aubinet et al. 2003; Staebler and Fitzjarrald 2004; Feigenwinter et al. 2004; Finnigan and Belcher 2004; Katul et al. 2006a; Aubinet et al. 2005; Foken et al. 2005), or estimating gene flow and dispersal patterns of pollen and seeds from nonflat ecosystems (Nathan et al. 2002; Soons et al. 2004; Nathan and Katul 2005; Katul et al. 2005, 2006b). Particularly, how complex terrain modulates the ejection-sweep cycle, which is the main coherent motion responsible for the bulk turbulent transport, remains a problem that has received surprisingly little attention. In contrast, studies on how hills modify the mean flow properties have received significant theoretical and experimental attention (e.g. see reviews in Finnigan 1988; Kaimal and Finnigan 1994; Finnigan and Brunet 1995; Belcher and Hunt 1998; Finnigan and belcher 2004). While the mean flow properties are strongly forced by the topography and can be plagued by 'discontinuities' such as separation or recirculation regions, it is not yet clear how the turbulence is affected by complex terrain. Early studies on flows above gentle hills suggest that such mean-flow discontinuities do not lead to concomitant discontinuities in the higher-order turbulence moments, at least in the absence of tall canopies (Finnigan 1988; Finnigan et al. 1990b). However, the main problem lies in the fact that turbulence 'remembers' a significant portion of the strain rate history injected by the mean flow, and the energy-containing eddies remember a significant portion of their relaxation history towards equilibrium. The relative importance of these two 'memories' can profoundly affect higher-order statistics across the hill and quantifying their interplay remains a vexing problem.

Progress on this problem is hindered by the absence of detailed experiments on the ejection-sweep cycle and higher-order statistics for flows inside (and above) canopies on gentle hills, and by the absence of simplified theories that readily connect the impact of these organized events to terms in the turbulent kinetic energy (TKE) budget equation. Another complication stems from the fact that surface roughness does play a significant role in the ejection-sweep cycle. Numerous experiments on flat terrain have already shown that while ejections dominate momentum transfer above a bare terrain, inside and just above dense canopies, sweeps dominate (Raupach 1981;

Shaw et al. 1983; Katul et al. 1997a; Finnigan 2000; Poggi et al. 2004b). Hence, the modulation of organized motion by topography cannot be studied in isolation from the surface cover. For vegetated surfaces, such modulations are likely to impose significant variability in the canopy sublayer thickness and perhaps even blur its basic definition.

Here, we present two new flume experiments that explore the higher-order turbulence statistics on a train of hills above a bare (almost smooth) surface and a vegetated surface composed of densely arrayed rods. Other processes such as unsteadiness in the mean flow conditions, density gradients, variability in canopy morphology (both horizontal and vertical), steep slopes and multiple modes of terrain variability can limit the immediate extrapolation of these flume experiments to field conditions; however, exploring all of these effects simultaneously is well beyond the scope of a single study.

Hence, the compass of this work is restricted to the connection between the ejection-sweep cycle and the higher-order statistics across various positions above a train of gentle hills with a 'lens' on the flux-transporting terms, the terms most affected by ejections and sweeps in the TKE budget. The tall forested experiment is designed such that the topographic variations remain comparable to the canopy height so that the interplay between organized eddy motion dominating canopy turbulence and the terrain variability is amplified (Finnigan and Belcher 2004).

2 Experimental set-up

The experiments were conducted in the OMTIT recirculating channel at the Giorgio Bidone hydraulics laboratory, DITIC Politecnico di Torino, Torino, Italy. The flume has a 18 m long, 0.9 m wide, and 1 m deep working section (see Fig. 1), and a recirculating flow rate up to $360\,\mathrm{l\,s^{-1}}$. Two test sections were used to simulate the bare and the forested surfaces on a hill. In both test sections, the hill topography was reproduced using a removable wavy stainless steel wall composed of four modules, each representing a sinusoidal hill with a shape function given by

$$\tilde{f}(X) = (H_\mathrm{h}/2)\ \cos(kX + \pi), \tag{1}$$

where X is the longitudinal distance, $H_\mathrm{h} = 0.08\,\mathrm{m}$ is the hill height, $k = \pi/(2L)$ is the hill wavelength with $L = 0.8\,\mathrm{m}$ being the half length shown in Fig. 2. The forest canopy is composed of an array of vertical stainless steel cylinders having a diameter of 4 mm ($= d_r$) and a height of $100 \pm 2\,\mathrm{mm}$ ($= H_\mathrm{c}$). The rods were firmly arc-welded into the stainless steel sheets at equal spacing along the 12.8 m long and 0.9 m wide test section. The rod density, $675\,\mathrm{rods\,m^{-2}}$, was shown to be sufficiently dense to resemble dense forested canopies (Poggi et al. 2004b). The vertical distribution of the rods' frontal area is not constant with height but is designed to resemble a tall hardwood canopy with its foliage concentrated in the top third and almost constant in the bottom two-thirds (see Fig. 1).

The velocity measurements were acquired along a predefined grid following a streamline coordinate system. Although several coordinate systems are possible (e.g. rectangular Cartesian or terrain following), a streamline coordinate system in which the coordinates are allowed to adjust according to the hypothetical flow dynamics are preferred. This system has the advantage of a displaced coordinate system because it reduces to a terrain-following system near the ground, and to a rectangular Cartesian

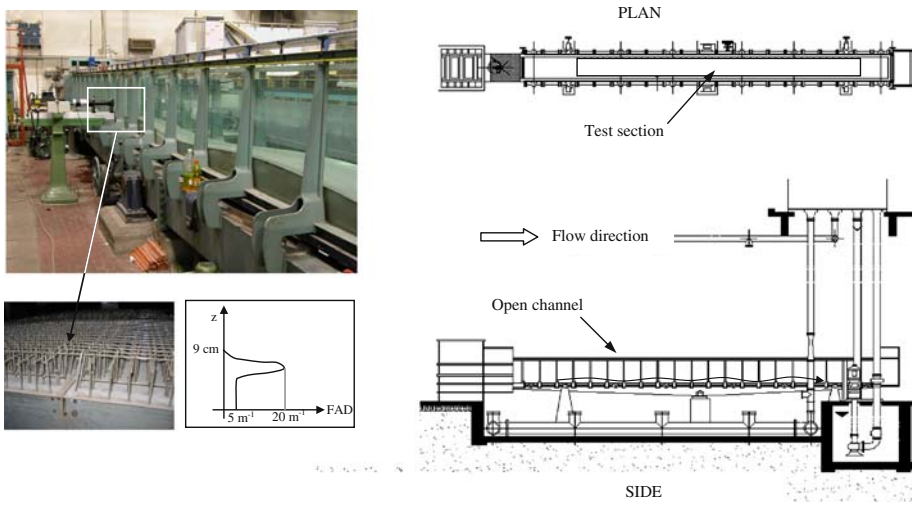

Fig. 1 The experimental set-up: Plan and side views of the flume and test sections (top and bottom right), the train of hills with the bare surface (top left), the model canopy composed of densely arrayed rods (bottom left), and the measured frontal area density (FAD) profile (analogous to a leaf area density profile in canopy turbulence)

system well above the hill. Hence, it retains the advantages of both coordinate systems in the appropriate regions (Finnigan and Belcher 2004). With respect to a rectangular coordinate system (X and Z) and for the hill shape function in Eq. 1, the displaced coordinates, to a leading order in the terrain slope, are given by

$$x = X + (H_h/2)\ \sin(kX)e^{-k(Z+H_c)}, \tag{2}$$

$$z = Z - (H_h/2)\ \cos(kX)e^{-k(Z+H_c)}, \tag{3}$$

where $H_c = 0$ for the bare surface. Note that the physical ground of the sinusoidal hill covered with the canopy is described by $Z_g = (1/2)H_h \cos(kX) - H_c$ in the rectangular coordinate system and, to a leading order, by $z_g = -H_c$ in the displaced coordinate system (Fig. 2).

The velocity time series were acquired using two-component laser Doppler anemometry (LDA). The velocity measurements were performed at 10 positions to longitudinally cover one hill module, and at 0.40 m from the lateral wall in the spanwise direction. These measurements were performed along 35 vertical positions in the streamlines coordinate system covering about 0.35 m of the 0.6 m water level. Here, we concentrated the vertical measurements near the surface to zoom onto the inner layer and canopy layer dynamics (Fig. 2).

The longitudinal (u) and vertical (w) velocity time series were measured above the third hill module. To check whether the turbulence was completely developed, preliminary measurements were conducted on the second, third, and fourth sections. These preliminary measurements showed that the velocity statistics acquired at four locations (and 10 vertical positions) around the crest of the second and the fourth hills do not significantly differ from their analogous statistics at the crest of the third hill. During the experimental planning phase, we conducted model calculations using

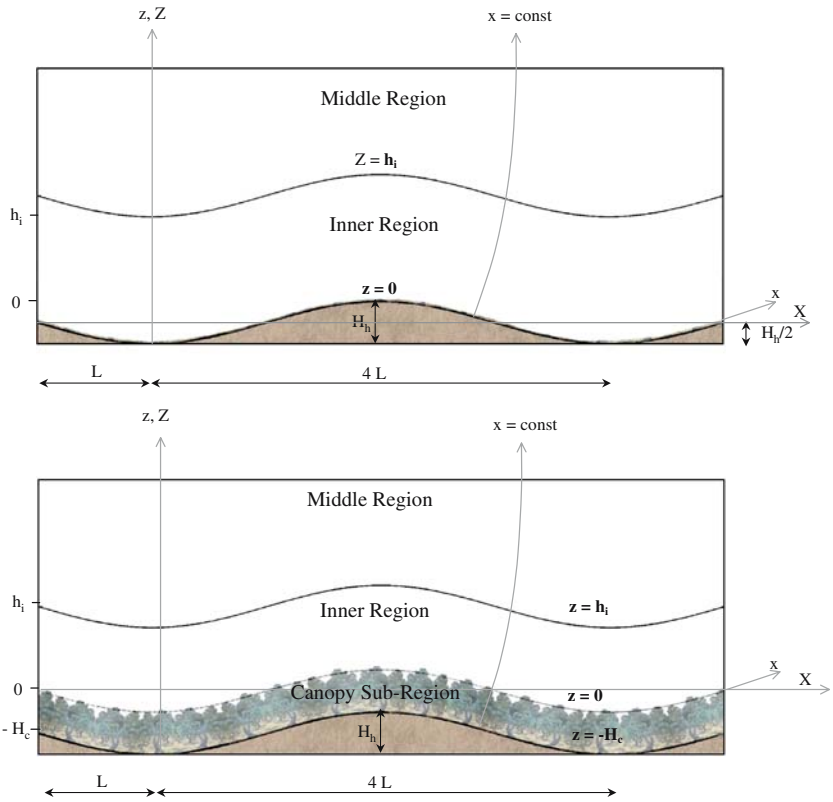

Fig. 2 The definition of the displaced coordinate (x, z) system for bare (top panel) and vegetated surfaces (bottom panel) in relation to the canopy height (H_c) and hill dimensions (H_h, L). The inner region depth (h_i) and the canopy sublayer region are also shown for reference

first-order closure principles and found that the mean velocity statistics above the third hill do not differ from their counterpart above the fourth hill as well.

The velocity measurements were conducted at a bulk Reynolds number $Re_b > 1.5 \times 10^5$, where Re_b is defined using the depth-averaged velocity and the water level ($= 0.6$ m). The sampling duration and frequency for each sampling position were 300 s and 2500–3000 Hz, respectively. Further details about the data acquisition, processing, and quality checks (including lateral homogeneity in the flow statistics around the sampling locations) can be found in Poggi et al. (2002).

At this Re_b, the bare surface case is not completely rough. In fact, for the bare surface case, the roughness Reynolds number $z_o^+ = u_* z_o/\nu = 36$ where $u_* = 0.018\,\mathrm{m\,s^{-1}}$ is the friction velocity ($u_* = 0.044\,\mathrm{m\,s^{-1}}$ for the vegetated case), ν is the kinematic viscosity, and $z_o = 2$ mm is the momentum roughness length of the hill surface. Here u_* is defined as the time-spatially averaged Reynolds stress at $z = 0$ (i.e. $u_*^2 = - < \overline{u'w'} > |_{z=0}$) for both the bare and the vegetated cases. The region in which $4 < z_o^+ < 60$ is classically referred to as dynamically slightly rough (Monin and Yaglom 1971); however, it is important to point out that $z_o^+ = 36$ is not significantly far from the fully rough region. Unless otherwise stated, $< \overline{c} >$ is the time and planar averaging of any flow variable c and $c' = c - < \overline{c} >$ (Raupach and Shaw 1982). While

planar averaging is only required in the canopy sublayer, we retain this notation for completeness in the theoretical development below.

3 Theory

The ejection-sweep cycle is often analyzed using conditional sampling methods and quadrant analysis applied to time series measurements of u' and w' (see review in Antonia (1981)). Quadrant analysis clusters each w' and u' event, collected at time t, into one of the four quadrants defined by the Cartesian plane whose abscissa and ordinate are u' and w', respectively. The quadrants reflect different modes of momentum transfer with quadrants II ($u' < 0$ and $w' > 0$) and IV ($u' > 0$ and $w' < 0$) representing ejections and sweeps respectively, and quadrants I ($u' > 0$ and $w' > 0$) and III ($u' < 0$ and $w' < 0$) representing outward and inward interactions, respectively. The latter two quadrants have no discernable contributions to the mean momentum flux $< \overline{u'w'} >$, at least when evaluating contributions originating from organized eddy motion. For such a quadrant representation, Nakagawa and Nezu (1977) and Raupach (1981) showed that the imbalance in momentum transfer between sweeps and ejections can be expressed as

$$\Delta S_o = \frac{\langle \overline{w'u'} \rangle|_{\mathrm{IV}} - \langle \overline{w'u'} \rangle|_{\mathrm{II}}}{\langle \overline{u'w'} \rangle}, \tag{4}$$

where $\langle \overline{w'u'} \rangle|_{\mathrm{IV}} / \langle \overline{u'w'} \rangle$ and $\langle \overline{w'u'} \rangle|_{\mathrm{II}} / \langle \overline{u'w'} \rangle$ are the stress fractions in quadrants IV and II, respectively.

To link ΔS_o and quadrant analysis with the TKE budgets and RANS models, we build on the pioneering work of Nakagawa and Nezu (1977) and Raupach (1981) in which the third-order cumulant expansion method (CEM) was successfully employed. Using a third-order CEM, Raupach (1981) showed that:

$$\Delta S_o = \frac{R_{uw} + 1}{R_{uw}\sqrt{2\pi}} \left[\frac{2C_1}{(1 + R_{uw})^2} + \frac{C_2}{1 + R_{uw}} \right], \tag{5}$$

where R_{uw}, C_1, and C_2 are given by

$$\begin{aligned}
R_{uw} &= \frac{\langle \overline{w'u'} \rangle}{\sigma_u \sigma_w}, \\
C_1 &= \left(1 + R_{uw}\right) \left[\frac{1}{6}(M_{03} - M_{30}) + \frac{1}{2}(M_{21} - M_{12}) \right], \\
C_2 &= -\left[\frac{1}{6}(2 - R_{uw})(M_{03} - M_{30}) + \frac{1}{2}(M_{21} - M_{12}) \right], \\
M_{ij} &= \frac{\langle \overline{w'^i u'^j} \rangle}{\sigma_w^i \sigma_u^j}; \quad \sigma_c = \sqrt{\langle \overline{c'c'} \rangle},
\end{aligned}$$

and where σ_c is the time and horizontally averaged standard deviation of any flow variable c. Using the above formulation, Katul et al. (1997a) conducted a sensitivity analysis on the relative importance of the mixed moments and the velocity skewness on ΔS_o. They demonstrated that the mixed moments M_{12} and M_{21} contribute much more to ΔS_o than M_{03} and M_{30}. Hence, based on this finding, Katul et al. (1997a) suggested a further simplification given by

$$\Delta S_o \approx \frac{1}{2R_{uw}\sqrt{2\pi}}\left[M_{21} - M_{12}\right], \tag{6}$$

and hereafter is referred to as an incomplete CEM (ICEM). Poggi et al. (2004b), Cava et al. (2005), and Fer et al. (2004) all reported excellent agreement between ICEM modelled and measured ΔS_o for boundary-layer and canopy flows on flat terrain. How well CEM and ICEM reproduce ΔS_0 on gentle hills remains largely unexplored.

To determine M_{12} and M_{21} within the context of RANS, closure models for $\langle\overline{w'u'w'}\rangle$ and $\langle\overline{w'u'u'}\rangle$ are needed. In general, RANS uses standard gradient-diffusion approximations for the momentum transport terms $\langle\overline{u_i'u_j'u_k'}\rangle$ given by

$$\langle\overline{u_i'u_j'u_k'}\rangle = q\lambda_1\left[\frac{\partial\langle\overline{u_i'u_j'}\rangle}{\partial x_k} + \frac{\partial\langle\overline{u_k'u_j'}\rangle}{\partial x_i} + \frac{\partial\langle\overline{u_i'u_k'}\rangle}{\partial x_j}\right], \tag{7}$$

where $q^2 = \langle\overline{u_i'u_i'}\rangle$ is twice the TKE, and λ_1 is a typical mixing length (Wilson and Shaw 1977). The two transport terms needed in Eq. 6 can then be expressed as

$$\langle\overline{w'u'w'}\rangle = q\lambda_1\left[2\frac{\partial\langle\overline{u'w'}\rangle}{\partial z} + \frac{\partial\langle\overline{w'w'}\rangle}{\partial x}\right], \tag{8}$$

$$\langle\overline{w'u'u'}\rangle = q\lambda_1\left[\frac{\partial\langle\overline{u'u'}\rangle}{\partial z} + 2\frac{\partial\langle\overline{u'w'}\rangle}{\partial x}\right]. \tag{9}$$

Belcher and Hunt (1998) argued that for the inner layer above a gentle hill, horizontal derivatives of *turbulent* quantities play a minor role in the closure of the momentum transport terms when compared with their vertical counterparts. Moreover, Finnigan and Belcher (2004) showed that, within a tall canopy covering a gentle hill, the horizontal derivatives scale with L while the vertical derivatives scale with the vortex size that is proportional to the mixing length l imposed by the canopy. Because l is a fraction of H_c, which is much smaller than L for gentle hills, horizontal derivatives of turbulent quantities can also be neglected inside the canopy. Extending the Belcher–Hunt and the Finnigan–Belcher inner-layer scaling arguments to higher-order turbulent quantities, the second-order closure model for ΔS_o reduces to

$$\Delta S_o = \frac{-1}{2\sqrt{2\pi}}\frac{q\lambda_1}{\langle\overline{w'u'}\rangle}\left[\frac{1}{\sigma_u}\frac{\partial\langle\overline{u'u'}\rangle}{\partial z} - \frac{2}{\sigma_w}\frac{\partial\langle\overline{w'u'}\rangle}{\partial z}\right]. \tag{10}$$

A comparison between measured and modelled ΔS_o using Eq. 10, forced by measured $<\overline{u'u'}>$, $<\overline{w'w'}>$, and $<\overline{u'w'}>$, provides an explicit evaluation of whether the ejection-sweep cycle is in *local equilibrium* with the vertical gradients of the second moments. However, to use Eq. 10, the characteristic length scale λ_1 must be defined. Poggi et al. (2004a, 2006) showed that for a dense canopy, λ_1 can be parameterized as

$$\lambda_1 = \begin{cases} \alpha H_c; \frac{z}{H_c} < d + \frac{\alpha H_c}{k_v} \\ \\ k_v(z-d); \frac{z}{H_c} > d + \frac{\alpha H_c}{k_v} \end{cases}$$

where $k_v = 0.4$ is the von Karman constant, d is the zero-plane displacement height, and α is a constant that depends on the drag and canopy leaf area density. In Poggi et al. (2004a), it was shown that this mixing length model does have some theoretical

basis inside canopies and outperforms models that use a constant Lagrangian time scale. Furthermore, Katul et al. (2004) demonstrated that closure approaches that use this λ_1 model even predict the TKE dissipation rate better than standard K–ϵ models. In Poggi et al. (2004a) and Katul et al. (2004), an $\alpha = 0.2$ was derived for flat terrain (and is adopted here). For the bare surface case, $\lambda_1 = k_v z$ is assumed for the entire inner layer. We note that Eq. 10 may be more robust to the gradient-diffusion approximation than Eq. 7, which is known to fail even for idealized atmospheric conditions (see Appendix for further discussion).

Equation 10 suggests that the adjustment of the second-order moments to the hill surface is intimately connected with the relative importance of ejections and sweeps across the hill, which can be explored via standard time scale arguments. In particular, Belcher and Hunt (1993) proposed the mean distortion (TD) and the Lagrangian integral (TL) time scales as tools to explore how the mean flow and turbulence adjust to changes in topography. TD characterizes the distortion of turbulent eddies due to the straining motion associated with spatial variability in the mean flow caused by the hill, and it represents the characteristic time that the mean flow field needs to stretch and destroy large eddies through work done by advection against the mean spatial velocity gradients. TL characterizes the time scale of the classical vortex stretching (or relaxation) of large eddies due to the action of a local mean-flow velocity gradient. Stated differently, TL is the time that turbulent fluctuations need to reach equilibrium with the local mean velocity gradient (Tennekes and Lumley 1972). This turbulence memory also represents the characteristic eddy turnover time contributing most to the magnitude of $\overline{w'u'}$, $\overline{w'w'}$, and $\overline{u'u'}$.

When TD/TL $<< 1$, the local stretching of large eddies is fast enough to compete with the distortion by the mean flow. This region is called the *local-equilibrium region* (or inner region) because the local eddies relax to equilibrium with the local mean velocity gradient before spatial advection can transport and stretch them. In this region, the turbulent time scale can be derived based on a local balance between the production and dissipation mechanisms. Hence, in a first-order analysis, the memory (or the relaxation time scale) of $\overline{w'u'}$, $\overline{w'w'}$, and $\overline{u'u'}$ may be estimated from the ratio of the magnitude of the flow variable to its dissipation rate. Moreover, the dissipation rate should be comparable to the production (P) term, given by

$$P_{uu} = \overline{w'w'}\,\partial\overline{u}/\partial z, \tag{11a}$$

$$P_{ww} = \overline{w'w'}\,\partial\overline{w}/\partial z, \tag{11b}$$

$$P_{wu} = \overline{w'u'}\,\partial\overline{u}/\partial z. \tag{11c}$$

From the continuity equation, $|\partial\overline{w}/\partial z| \sim |\partial\overline{u}/\partial x|$; hence, the relaxation time I of $\overline{w'u'}$, $\overline{w'w'}$, and $\overline{u'u'}$ are

$$I_{uw} = \frac{\overline{w'u'}}{\overline{w'w'}}\left(\frac{\partial\overline{u}}{\partial z}\right)^{-1}, \tag{12a}$$

$$I_{ww} = \frac{\overline{w'w'}}{\overline{w'w'}}\left(\frac{\partial\overline{u}}{\partial x}\right)^{-1}, \tag{12b}$$

$$I_{uu} = \frac{\overline{u'u'}}{\overline{w'u'}}\left(\frac{\partial\overline{u}}{\partial z}\right)^{-1}. \tag{12c}$$

While I_{uw} and I_{uu} are proportional to $\partial\overline{u}/\partial z^{-1}$, I_{ww} scales with $\partial\overline{u}/\partial x^{-1}$. This time scale argument may suggest that $\overline{u'u'}$ and $\overline{w'u'}$ adjust rapidly to changes in local

boundary conditions (and hence vary significantly across the hill) while $\overline{w'w'}$ might require much longer time to adjust to changes in topography. When these scale arguments are taken in the context of Eq. 10, the equilibration time scale of ΔS_o with topography is likely to be comparable to I_{uw} or I_{uu} rather than I_{ww}. The data collected here will permit us to explore these scaling arguments.

4 Results

We first show the longitudinal and vertical variations of both lower and higher-order flow statistics for the two surfaces and then proceed to show the model comparisons of the flux-transport terms, the skill of CEM and ICEM in reproducing ΔS_o, and the adequacy of Eq. 10 for the inner layer. Our main objective for presenting both lower- and higher-order velocity statistics here are twofold: (1) to provide a bench-mark dataset on the fundamental statistics of canopy and boundary-layer flows on gentle hills, and (2) to investigate the joint effects of topography and surface cover on the basic variables known to influence the ejection-sweep cycle in the inner layer. Formally, the inner layer depth (h_i) can be estimated by solving the nonlinear equation (e.g. Finnigan and Belchen 2004; Belcher and Hunt 1998)

$$\frac{h_\mathrm{i}}{L} = \frac{2k_\mathrm{v}^2}{\ln(h_\mathrm{i}/z_0)}, \tag{13}$$

where z_o is the aerodynamic roughness length of the hill surface, and L is, as before, the hill half-length. The inner layer region is defined as the region for which $z/h_\mathrm{i} < 1$, and the canopy sublayer is the region immediately impacted by the canopy and spans about $-H_\mathrm{c} < z < 0$.

4.1 Lower-order statistical moments

4.1.1 Mean velocity distribution

In Fig. 3, we show the mean velocity profiles for both smooth and vegetated cases. While the left panels (3a, c) show the measured spatial patterns of $\overline{u}$ across the hill surface along with the inner region, the right panels (3b, d) show the velocity profiles measured at the 10 sections marked in Figs. 3a, c (s1–s10). Note that here the overbar indicates temporal averaging, and the brackets indicates spatial averaging over the 10 profiles.

From Figs. 3a, c, a well-defined feature inside the canopy on the lee side of the hill is an apparent recirculation region, a region where $\overline{u} < 0$ and is delineated with a continuous line in panel 3a; it is also noticeable in panel 3b. This region, predicted to occur because of the interplay between the mean longitudinal pressure gradient and the nonlinear drag force (Finnigan and 2004; hereafter referred to as FB04), has no analogue for the bare surface case despite the similarity in topographic variability and mean flow conditions. However, the spatial extent of this region is smaller than that reported in FB04 (see also Katul et al. 2006a).

To compare the spatial patterns of the mean flow field for bare and vegetated surfaces, we redefine the inner region depth in a new and spatially explicit manner. This is needed because the standard definition of h_i does not account for any spatial variability in the flow field. Here, we define the *dynamical inner region* depth as the

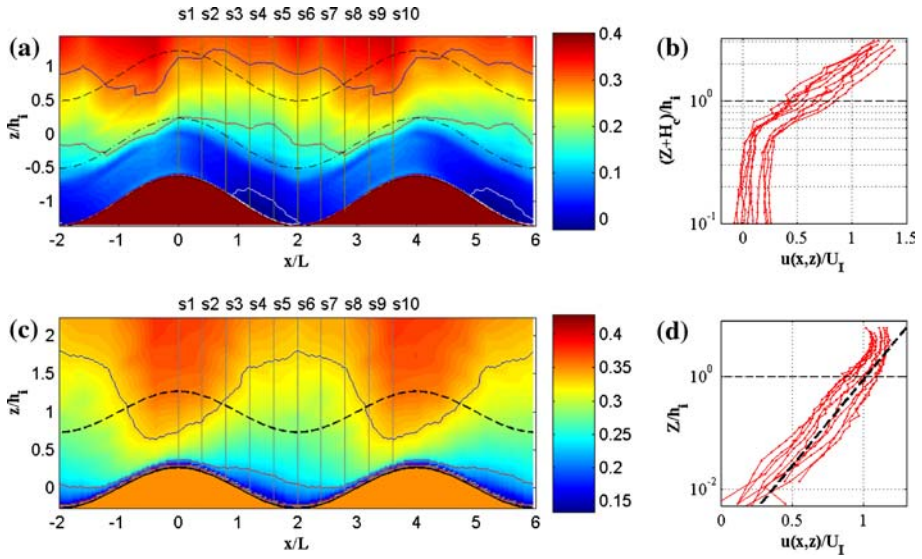

Fig. 3 (*Left panels*) The measured spatial variation of longitudinal velocity u for the vegetated surface (top panel) and the bare surface (bottom panel) along the hill. The colours represent the variation of the actual (or *non normalized*) values of u (in m s^{-1}). The longitudinal distance x is normalized by the hill half-length L and the vertical distance z is normalized by the inner layer height h_i. The mean inner layer depth (dotted line) and canopy top (dash-dotted line) are also shown for reference with respected to the ground. The recirculation region, defined as the region for which the mean velocity < 0, inside the canopy near the bottom on the lee-side of the hill is also highlighted for clarity. The dynamical inner region and ground, defined as the height at which the measured $\overline{u}$ matches the mean u at $z = h_i$ and $z = 0.05h_i$, are also shown (blue and red continuous line respectively). (*Right Panels*): The measured profiles of normalized u for the vegetated surface (top panel) and bare surface (bottom panel); the sampling positions of the 10 profiles are marked in the left panels as s1–s10 . These u profiles for the vegetated and bare surfaces are normalized by their background state defined at the canopy top and at the inner layer height, respectively

distance from the ground where the measured local velocity is identical to the spatially averaged velocity at h_i (i.e. $\overline{u} = <\overline{u}>|_{z=h_i}$). This region is delineated in Figs. 3a, c by a continuous line. The longitudinal variability of this dynamical inner region for both surfaces shows a common asymmetric pattern with respect to the hill surface. Likewise, when this analysis is repeated for the canopy top and in the region close to the ground for the bare surface case, a new and dynamically based virtual ground can be defined. The canonical pattern of this virtual ground is shared by the flows over the bare and vegetated surfaces (continuous line in Figs. 3a, c). In particular, the flow accelerates in the upwind side and decelerates on the lee side for both surface covers in an asymmetric manner. While a recirculation region does not exist in the case of a bare surface on the lee side of the hill, the region below this virtual ground region exhibits very low velocity values that can affect the higher-order statistics.

From Figs. 3b, d, it can be noted that in the upper part of the inner layer, the mean velocity profiles above both surfaces approach a logarithmic shape. However, in the lower levels of the inner layer, the $\overline{u}$ for the forested surface is strongly sheared near the canopy top and is almost invariant with z well inside the canopy (though varying significantly with x), not entirely consistent with the assumptions in FB04.

4.1.2 Shear stress distribution

In Fig. 4, the shear stress profiles, $\tau = -\overline{u'w'}$, for both forested and bare surfaces, are shown together. In the inner layer, the variations of τ for the bare surface case when normalized by u_* are close to the vegetated surface only for the first four profiles (s1–s4) but they diverge at the bottom of the hill and for the upwind side (s5–s9). In fact, when comparing the longitudinal variation of normalized τ from these two experiments, the overall spatial variation is much larger for the bare surface case. The peak of τ occurs at heights even exceeding the inner layer depth for the upwind sections (s6–s8) for the bare surface case.

Inside the canopy, the drag dampens $|\mathrm{d}\overline{u'w'}/\mathrm{d}x|$ but amplifies $|\mathrm{d}\overline{u'w'}/\mathrm{d}z|$. Note that the apparent recirculation region (Fig. 3, s4–s5) has little 'signature' in the $\overline{u'w'}$ spatial distribution of the forested surface. This is an important and surprising finding. While the apparent recirculation region strongly affects the mean flow field, it does not dramatically alter the canonical profiles of the Reynolds stress and, as we demonstrate later, other higher- order moments. Although this result seems counterintuitive, further analysis carried out using a special visualization technique (Laser Induced Florescence or LIF, see Poggi et al. 2006) revealed that the apparent recirculation is not due to a continuous 'rotor' but to an alternating flow that switches asymmetrically between positive and negative velocity. This asymmetry in the switching, when time-averaged, leads to a negative velocity and an apparent recirculation region. Because

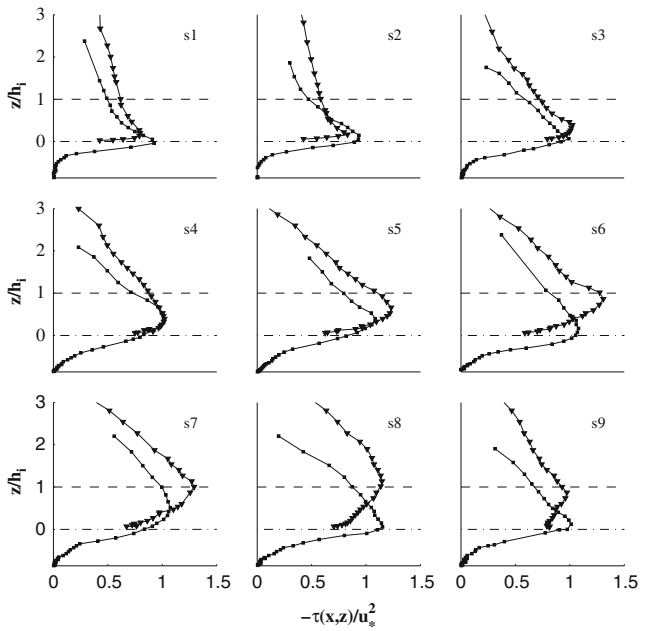

Fig. 4 Variation of the Reynolds stress, $-\overline{u'w'} = \tau$, for the bare surface (triangle) and vegetated surface (square) along nine of the ten vertical sampling positions, labelled as s1–s9 (see left panels of Fig. 3 for positions of these vertical sections across the hill). The horizontal lines are the inner layer depth (top line) and the canopy height (bottom line). Recall that sections s4 and s5 sample the recirculation region in the canopy case

a persistent vortex does not exist in this region, the turbulent statistics appear less affected by the alternating motion when compared to the mean flow.

4.1.3 Velocity variances distribution

Figure 5 shows the normalized longitudinal ($\sigma_u^+ = (\overline{u'u'})^{0.5}/u_*$) and vertical standard deviation profiles ($\sigma_w^+ = (\overline{w'w'})^{0.5}/u_*$) for the vegetated surface. Likewise, Fig. 6 shows the vertical profiles of σ_u^+ and σ_w^+ for the bare surface (s1–s9). When comparing Figs. 5 and 6, the first-order effect to explain the difference between the two experiments remains the attenuation of the flow statistics within the canopy volume irrespective of the position on the hill. In particular, it is evident that, while the magnitude of σ_w^+ for the bare and vegetated cases are close, σ_u^+ is strongly affected by the canopy. In fact, the maximum values of σ_u^+ for the vegetated surface are smaller than their counterpart for the bare surface. As with the shear stress, the apparent recirculation region has no discernable fingerprints (Fig. 3) in these two moments.

Well inside the canopy (except very close to the ground), the ratio of σ_u^+ to σ_w^+ for the vegetated case tends to unity suggesting that the flow approaches an 'sisotropic' state. This tendency towards isotropy seems to be mildly sensitive to topographic variation. Note that the isotropy for the vegetated case is not a surprising result. Similar results have been reported for flat surfaces (e.g. Poggi et al. 2004b) and within a uniform pine forest (e.g., see Katul and Chang 1999). These studies attributed the approach to isotropy to the weakening of the mechanical production of TKE in these

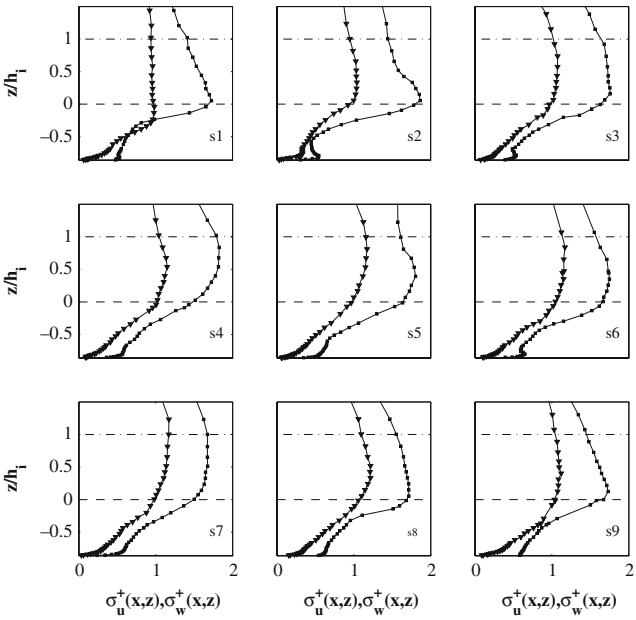

Fig. 5 The vertical profiles of longitudinal (square) and vertical (triangle) velocity standard deviation for the vegetated surface, $\sigma_u^+ = \overline{u'^2}^{1/2}/u_*$, and $\sigma_w^+ = \overline{w'^2}^{1/2}/u_*$ respectively. As in Fig. 4, the canopy top and inner layer depth are highlighted by the dash-dot and dashed lines respectively

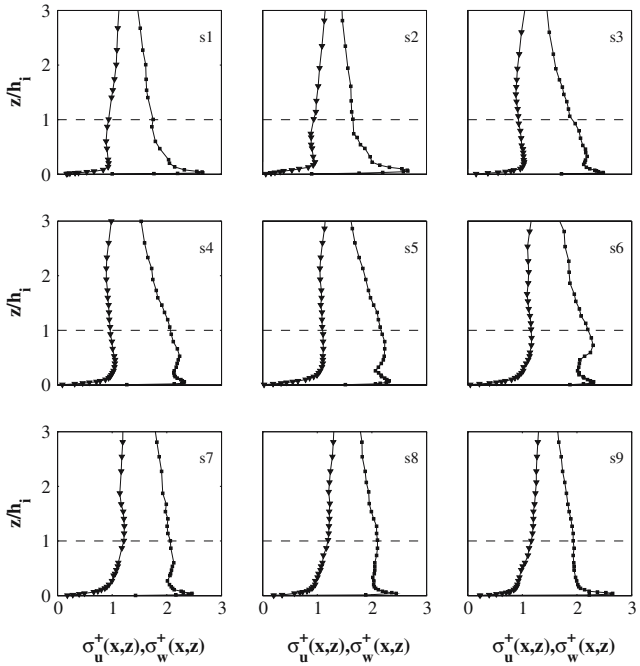

Fig. 6 Same as Fig. 5 but for the hill covered with the bare surface

deeper layers (one of the main sources of anisotropy production) and the increased role of the pressure-transport terms that have a return-to-isotropy component.

From Figs. 4, 5, and 6, we find that σ_w^+ does not vary appreciably across the hill when compared to σ_u^+, which is consistent with the time-scale arguments presented in the theory section. In fact, this time-scale argument correctly predicted that $\overline{w'w'}$ may require a much longer time to adjust to changes in topography when compared to $\overline{u'u'}$ within the inner layer. Recall that Eq. 10 suggests that the equilibration time scale of ΔS_o is likely to resemble I_{uu} rather than I_{ww}. However, before exploring the spatial variations in ΔS_o based on the second-order closure models, we consider the spatial variations of the triple moments first for three reasons: (1) the velocity skewnesses are often used as indicators of the imbalance between ejections and sweeps, and (2) the CEM and ICEM expansions of ΔS_o require these triple moments, and (3) the predictive skills of the gradient-diffusion closure at various positions across the hill can be tested.

4.2 Triple moments and gradient-diffusion closure

Because the degree of asymmetry in the probability density function is an elementary indicator of the strength of the ejection-sweep cycle, we show the variation in the skewness of u (Sk_u) and w (Sk_w) along the hill for both surfaces in Figs. 7 and 8.

In the upper part of the inner layer, the Sk_u and Sk_w are comparable in both magnitude and sign above both surfaces confirming the results derived from lower-order moments. However, in the lower part of the inner region, the magnitudes of Sk_u and

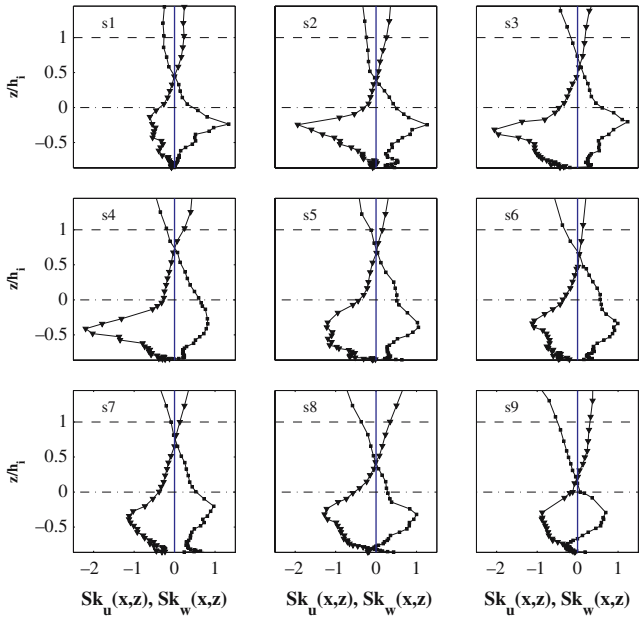

Fig. 7 Same as Fig. 5 but for the longitudinal and vertical velocity skewness ($Sk_u = \overline{u'^3}/\sigma_u^3$ and $Sk_w = \overline{w'^3}/\sigma_w^3$)

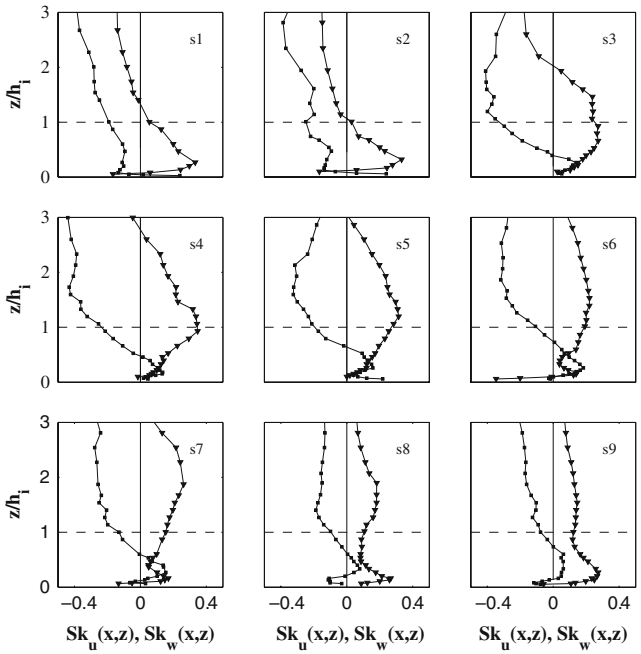

Fig. 8 Same as Fig. 7 but for bare surface case

Sk_w are much larger for the forested surface (Fig. 7) when compared to their bare surface counterpart (Fig. 8) suggesting that the ejection-sweep cycle is more intense for the forested surface. We use the term more intense (in Sk) to imply that the degree of asymmetry in the probability density function, as measured by the magnitude of the skewness, is larger. As shown by Poggi et al. (2004a,b), the magnitudes of both Sk_u and Sk_w within the canopy increase with increasing canopy density. The positive Sk_u and the negative Sk_w in Figs. 7 and 8 also suggest an extensive region within and just above the canopy that is dominated by sweeps along the hill. While the thickness of this 'sweep' dominated region is longitudinally variable (Fig. 7), it is always larger than the canopy height, perhaps suggesting a new method to define or identify the vertical extent of the canopy sublayer. This region is generally deeper on the lee side of the hill and shallower near the hill top. This effect is largely linked with the virtual ground presented in Fig. 3. In fact, as shown in Fig. 3a, the dynamical ground is much thinner at the top of the hill but becomes deeper above the bottom of the hill. We will check whether these results are consistent with the spatial variations of ΔS_o in the following section.

The analysis in Figs. 7 and 8 are repeated for the triple moments $\overline{w'u'u'}$ and $\overline{w'u'w'}$ for both vegetated (Fig. 9) and bare surfaces (Fig. 10). For both surfaces, the magnitude and sign of these flux transport terms are similar near the top of the inner layer consistent with the skewness comparisons. The largest difference is observed in the lower layers of the inner region, where the sign of both mixed moments reverse and the magnitudes rapidly increase with decreasing distance from the ground. The fact that the largest flux-transport terms are measured above and within the forested surface and agrees with the skewness analysis (Fig. 7) further confirms the intensification of the ejection-sweep cycle. Note that, while these results are not qualitatively different from their flat-terrain counterpart, there is a clear topographic signature on the flux transport terms for both surface covers.

Figures 9 and 10 also show the transport terms modelled using the vertical-gradient diffusion closure (i.e. Eq. 10). For both surfaces, the agreement between measured and modelled quantities is surprisingly good (see Table 1 for regression statistics) despite the simplicity and one-dimensionality of this model. Using the data directly, we also verified that the longitudinal gradients in Eq. 9 and 10 are small when compared to their vertical counterparts at all positions within the inner layer. When taken together, these results hint that the argument put forth by Belcher and Hunt FB04 can be extended to the mixed moments. In fact, even within the apparent recirculation region identified in Fig. 3, the mixed moments are well-reproduced by a gradient-diffusion formulation (i.e. an equilibrium model).

Up to this point, we have qualitatively shown how the signature of the ejection-sweep cycle is modulated across the hill and surface cover. Next, a quantitative analysis is carried out using quadrant analysis and conditional sampling, CEM and ICEM, and gradient-diffusion arguments.

4.3 Measurements and models for ΔS_o

Figures 11 and 12 show how ΔS_o, derived from quadrant analysis for the forested and the bare surfaces, varies across the hill. For the forested surface (Fig. 11), sweeps dominate inside the canopy and the lower region of the inner layer while ejections dominate near the top of the inner layer. For the bare surface case (Fig. 12), ejections dominate across the entire inner layer, except for a thin region near the ground on

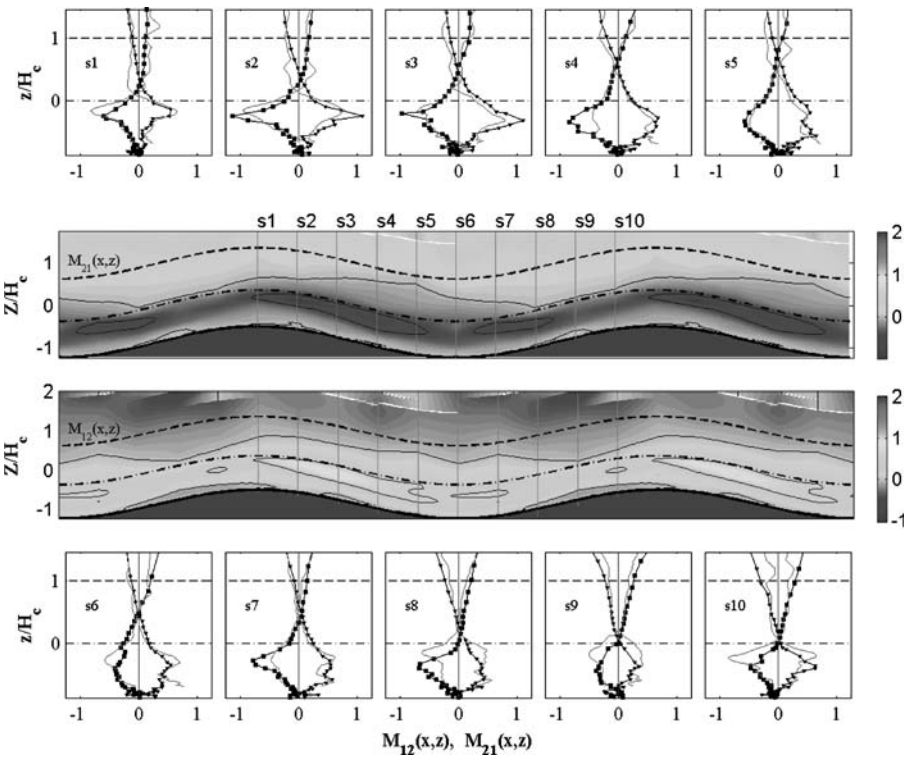

Fig. 9 The comparison between measured (symbols) and modelled (line) dimensionless turbulent transport terms $M_{12} = \overline{w'u'u'}/(\sigma_w\sigma_u^2)$ (square), and $M_{21} = \overline{w'u'w'}/(\sigma_w^2\sigma_u)$ (triangle), at each position on the hill covered with the vegetated surface. The sampling positions are labeled as s1–s10 and their locations with respect to the hill are presented in the two middle panels. These panels show the spatial patterns of M_{21} (top) and M_{21} (bottom). The dashed and dash-dot lines are the inner layer depth and the canopy height respectively

the lee side of the hill. Also, the magnitudes of ΔS_o are much bigger in the lower part of the inner region for the forested case when compared to the bare surface case, in agreement with the skewness analysis (Figs. 5, 6). Another important feature is the similarity in the spatial patterns of ΔS_o and the flux transport terms in the lower layers of the inner region. This similarity demonstrates the intimate links between ΔS_o and the flux transport terms across the hill, especially in the inner layer (as expected from the ICEM approach). Figure 11 also shows the intensification of sweeps on the lee side of the hill as alluded to in the flux-transport term analysis for the forested surface.

The spatial variations in ΔS_o offer a new possibility to define a dynamic canopy sublayer analogous to the virtual ground. Given that a defining feature of the canopy sublayer is the predominance of sweeps, the boundary line marking the transition from sweeps to ejections can be a logical choice in defining the local thickness of the canopy sublayer. From Fig. 11, it can be seen that this boundary line is not in phase with the topography in agreement with the virtual ground shown in Fig. 3. Whether there exists a connection between the virtual ground (or the canopy sublayer thickness) and the local pressure gradients needs to be explored using large-eddy simulations (Ross and Vosper 2005).

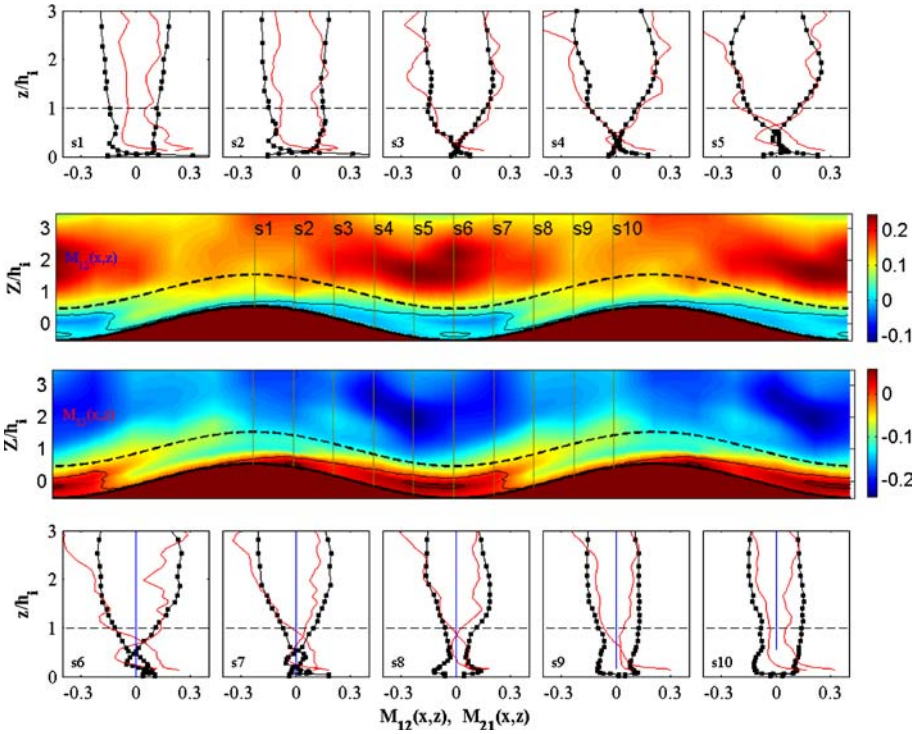

Fig. 10 Same as Fig. 9 but for the hill covered with the bare surface

Table 1 Comparison between measured (abscissa) and modelled (ordinate) flow variables across the entire hill in the inner layer. For ΔS_o, the models include CEM, ICEM, and the gradient-diffusion closure coupled with ICEM. The regression slope (α) and the correlation coefficient (R) are shown

Variable	Bare	surface	Canopy	Surface
	α	R	α	R
M21	0.71	0.68	0.79	0.86
M12	0.74	0.63	0.82	0.87
CEM	0.98	0.97	1.13	0.96
ICEM	1.01	0.98	0.93	0.94
Gradient- Diffusion	1.14	0.64	0.85	0.82

Figures 11 and 12 compare ΔS_o derived from quadrant analysis with ΔS_o computed using the CEM and the ICEM formulations (driven by measured M_{03}, M_{30}, M_{12}, and M_{21}). It is clear from this comparison that the CEM approach reproduces well the measured ΔS_o for both surfaces while the ICEM approach reproduced well (see Table 1 for regression statistics) the measured ΔS_o for the bare surface but marginally overpredicts the maximum magnitudes for the forested surface. It is obvious that this overprediction must be connected with the large M_{03} and M_{30} contributions (see Figs. 7 and 8) that are neglected in the ICEM formulation. Despite this

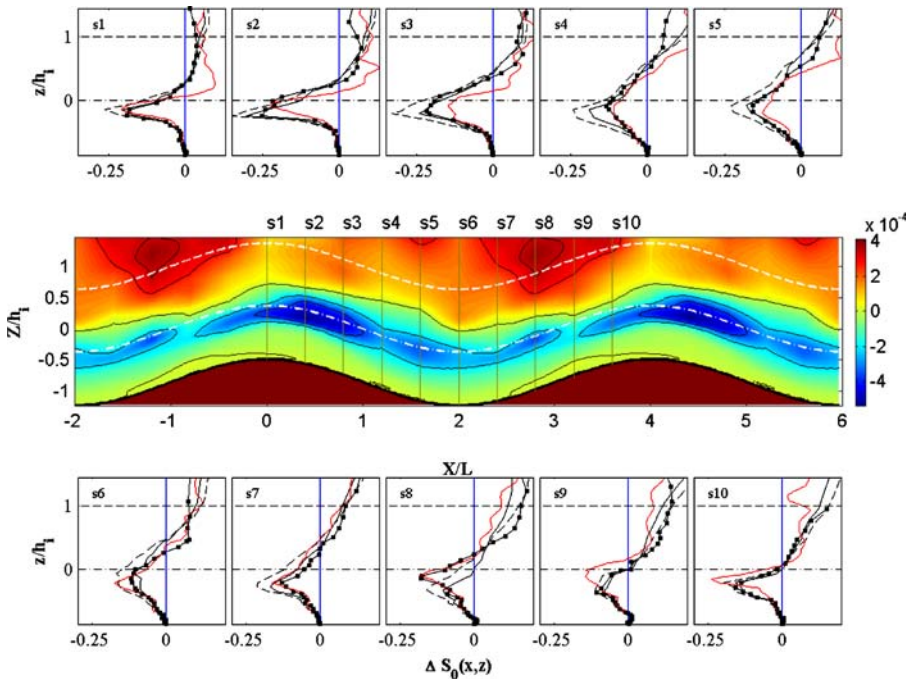

Fig. 11 Comparison between measured and modelled ΔS_o at each position on the hill covered with the vegetated surface. The symbols are for measurements via quadrant analysis, the solid line is for the complete CEM, and the dashed lines are the incomplete CEM or ICEM. The sampling positions are labelled as s1–s10 and their location with respect to the hill are presented in the middle panels. As in Fig. 9, these panels show the spatial pattern of the measured ΔS_o. Note that the middle panel (colour plot) represents $\Delta S_o = \langle \overline{w'u'} \rangle|_{\mathrm{IV}} - \langle \overline{w'u'} \rangle|_{\mathrm{II}}$ (i.e. in $\mathrm{m}^2\ \mathrm{s}^{-2}$) to contrast with the bare the surface. The dashed and dash-dot lines are the inner layer depth and the canopy height respectively

marginal overprediction, all the main features in the measured ΔS_o profiles were well reproduced by the ICEM approach.

Figures 11 and 12 also present the comparison between measured and modelled ΔS_o from the ICEM approach but using gradient-diffusion closure instead of the measured M_{12} and M_{21}. That is, ΔS_o is entirely computed from the assumed mixing length model and the local vertical gradients in the measured second-order moments shown in Figs. 4, 5, and 6. By and large, the comparison between measured and modelled ΔS_o is surprisingly good (see Table 1 for regression statistics) for the forested surface (in some regions, the agreement is even better than the original ICEM). For the bare surface case, the agreement between measured and modelled ΔS_o is degraded at least with respect to the ICEM or the CEM methods. Specifically, the model failure was rather significant near the top of the hill where the model predicted an unrealistically small ΔS_o. This failure is clearly attributed to the closure model not being able to reproduce the imbalance among the two flux transport terms in this region (see Fig. 10). A possible explanation is that as the mean flow switches from an accelerating to a decelerating phase, the advection should be taken into account in modelling the flux transport terms. With the exception of this region for the bare surface case, it is safe to say that the model does reproduce the impact of the hill on both the sign and

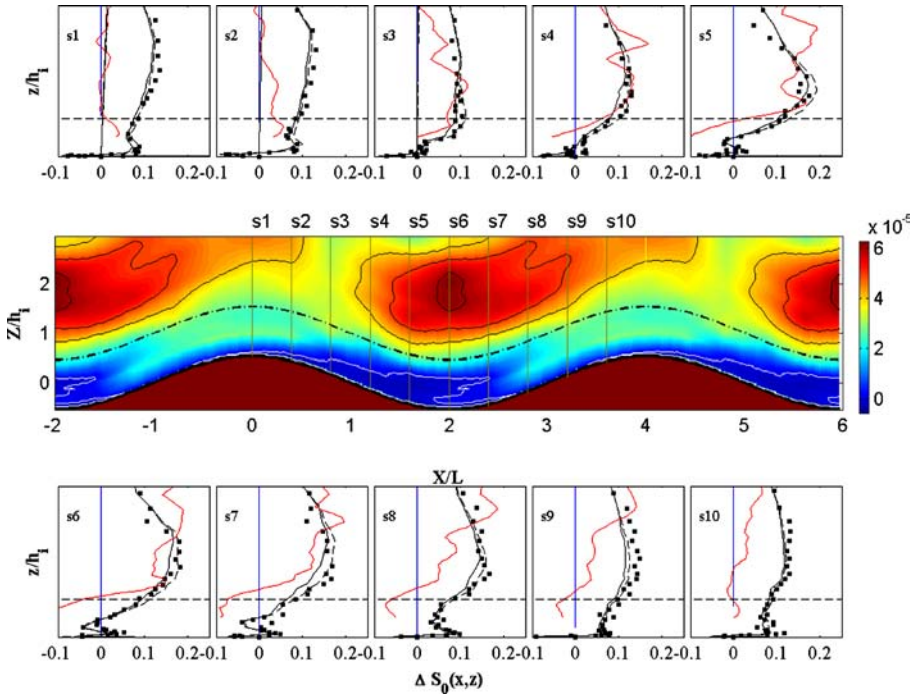

Fig. 12 Same as Fig. 11 but for the hill covered with the bare surface

the magnitude of ΔS_o (see Table 1). This agreement implies that the flux transport properties of the ejection-sweep cycle can be reproduced from the local gradients of the second moments via a one-dimensional model, at least for gentle hills irrespective of the surface cover.

5 Summary and conclusions

We presented the main turbulent flow statistics for forested and bare surfaces on a train of gentle hills in a large flume. This dataset is the first to explore the combined effects of hills and surface cover on higher-order statistics and the ejection-sweep cycle within the inner layer using ΔS_o, a measure of the relative contribution of ejections and sweeps to momentum transfer.

We showed that it is possible to infer the local variations of ΔS_o from standard flow statistics. Specifically, we found that the incomplete third-order cumulant expansion (ICEM) approach reproduced both the sign and magnitude of ΔS_o surprisingly well for the inner layer. When this finding is combined with standard gradient-diffusion closure principles, we showed that ΔS_o can be analytically linked to the gradients of $(\overline{u'w'})$, σ_u^2 and σ_w^2. Using both measured and modelled ΔS_o from vertical gradients of the second-order statistics, we showed that ejections dominate momentum transfer for both surface covers at the top of the inner layer. However, inside the canopy, sweeps dominate momentum transfer at all positions across the hill while ejections

remain the dominant momentum transfer mode over the bare surface. Moreover, sweeps also dominate momentum transfer above the canopy top though the thickness of this sweep-dominated region is longitudinally variable and is not in phase with the hill surface.

The broader impact of this study can be summarized as follows: if gradient-diffusion closure schemes for the triple moments do capture the statistical properties of the ejection-sweep cycle as shown by the ΔS_o comparisons here, then these ejection-sweep properties must be in local equilibrium with the local gradients of the second moments (even within the apparent recirculation region). Given that advection remains significant in the mean momentum equation, the only way this local equilibrium can be maintained here is when the time scales responsible for the production of ejections and sweeps are sufficiently shorter than the advection-distortion time scale by the mean velocity within the inner layer. This argument generalizes the time-scale argument for the mean momentum balance earlier put forth by Belcher and Hunt (1998). A practical consequence of this argument is that it is now possible to explore how various boundary conditions alter the properties of the ejection-sweep cycle by quantifying their impact on the gradients of the second moments.

While the proposed combination of gradient-diffusion and ICEM approaches was successful in predicting the sign and magnitude of ΔS_o for gentle hills and uniform canopies under steady-state neutral conditions, several limitations still remain. For example, whether this model can predict ΔS_o in the presence of large mean pressure gradients (e.g. steep topography), flows with a large stable density stratification, or when the horizontal heterogeneity length scale (e.g. forest edges) dominates the advective transport over short distances remains to be investigated. Nonetheless, this approach provides a simplified framework for beginning to confront these complex scenarios.

Finally, we showed that the sign of ΔS_o can be used as a logical indicator for 'marking' the region more affected by the canopy in complex terrain. Based on this assumption, we showed that the thickness of this region is not constant along the hill and not in phase with the topography. Recent large-eddy simulations suggest that the pressure is not in phase with topography perhaps hinting that a connection between the thickness of this region and the mean pressure may exist. If so, then ΔS_o can be used to define a virtual ground that replaces the topography in boundary-layer models. The canopy sublayer thickness (or virtual ground) is also useful in the design of experiments aimed at measuring biosphere-atmosphere exchange over complex terrain, and in the development of simplified models that aim at predicting the role of advection from prescribed pressure assumed to be in phase with topography.

Acknowledgements The authors acknowledge the support of the National Science Foundation (*NSF-EAR and NSF-DMS*), the Biological and Environmental Research (*BER*) Program, U.S. Department of Energy, through the Southeast Regional Center (*SERC*) of the National Institute for Global Environmental Change (*NIGEC*), and through the Terrestrial Carbon Processes Program (*TCP*) and the *FACE-FACTS* project.

Appendix: Robustness of the gradient-diffusion approximation for modelling ΔS_o

For flat and uniform terrain, several field experiments for the near-neutral atmospheric surface layer already reported a finite $\overline{w'w'u'}$ despite a near-constant $\overline{u'w'}$ (Kader and Yaglom 1990). A finite $\overline{w'w'u'}$ cannot be consistent with gradient-diffusion closure

predictions if $\mathrm{d}\overline{u'w'}/\mathrm{d}z = 0$. We explore in this Appendix how this inconsistency may propagate to ΔS_o predictions in Eq. 10. Katul et al. (1997b) found that $M_{12} \simeq 0.12$ rather than zero in the dynamic sublayer above a flat uniform bare soil surface and a tall grass surface consistent with the long-term surface-layer data reported in Kader and Yaglom (1990). Interestingly, Katul et al. (1997b) also found for the same experiments that (i) $M_{12} = M_{21}$ and (ii) $\Delta S_o = 0$ (via quadrant analysis). Hence, while a gradient-diffusion model erroneously predicts $M_{12} = M_{21} = 0$ (rather than 0.12), Eq. 10 correctly predicts $\Delta S_o = 0$.

Another check on Eq. 10 for rough and smooth-walled boundary layers comes from the wind-tunnel experiments of Raupach (1981). In these experiments, it was reported that $M_{21} \approx 0.73\Delta S_o$, $R_{uw} = -0.3$, and $M_{21} \simeq -M_{12}$ across the entire boundary layer (i.e. surface layer and outer layer). Using Eq. 10 and assuming $M_{12} \simeq -M_{21}$, we obtain $2M_{21} = -2R_{uw}(2\pi)^{1/2}\Delta S_o$, which results in $M_{21} = 0.75\Delta S_o$ for $R_{uw} = -0.3$. The predicted coefficient (= 0.75) from Eq. 10 is remarkably close to the value (= 0.73) reported by Raupach (1981). Note that these wind-tunnel experiments exhibited significant vertical gradients in the second moments, especially in the outer layer. When these two results are taken together, it is clear that ΔS_o predictions are not sensitive to the precise magnitudes of M_{12} and M_{21} but to the imbalance between them. When the gradients in the second moments are small, the imbalance is small, and Eq. 10 still captures the correct ΔS_o. When the gradients in the second moments amplify, gradient-diffusion estimates of the mixed moments improve, and Eq. 10 may still be a good predictor of ΔS_o.

We also show that Eq. 10 correctly predicts the 'intensification' of sweeps over ejections as canopy density increases (but for the same flow statistics) by noting that in a planar homogeneous flow, Eq. 10 can be expressed as

$$\Delta S_o = \frac{-1}{2\sqrt{2\pi}} \frac{q\lambda_1}{\langle \overline{w'u'} \rangle} \left[\frac{1}{\sigma_u} \frac{\partial \langle \overline{u'u'} \rangle}{\partial z} + \frac{2}{\sigma_w} C_\mathrm{d} a(z) \overline{u}^2 \right], \tag{14}$$

where C_d is the drag coefficient and $a(z)$ is the leaf area density. Hence, for the same flow statistics, when (C_d a) increases, ΔS_o also increases (positively) indicating that the role of sweeps is to intensify momentum transfer consistent with the flat-terrain measurements reported in Poggi et al. (2004b).

References

Antonia R (1981) Conditional sampling in turbulence measurement. Ann Rev Fluid Mech 13:131–156

Aubinet M, Heinesch B, Yarneaux M (2003) Horizontal and vertical CO_2 advection in a sloping forest. Boundary-Layer Meteorol 108:397–417

Aubinet M, Berbigier P, Bernhofer C, Cescatti A, Feigenwinter C, Granier A, Grunwald H, Havrankova K, Heinesch B, Longdoz B, Marcolla B, Montagnani L, Sedlak P (2005) Comparing CO_2 storage fluxes and advection at night at different CARBOEUROFLUX sites. Boundary-Layer Meteorol 116:63–94

Baldocchi D, Finnigan J, Wilson K, Paw U, Falge E (2000) On measuring net ecosystem carbon exchange over tall vegetation on complex terrain. Boundary-Layer Meteorol 96:257–291

Baldocchi D, Falge E, Gu LH, Olson R, Hollinger D, Running S, Anthoni P, Bernhofer C, Davis K, Evans R, Fuentes J, Goldstein A, Katul G, Law B, Lee X, Malhi Y, Meyers T, Munger W, Oechel W, Paw K, Pilegaard K, Schmid H, Valentini R, Verma S, Vesala T, Wilson K, Wofsy S (2001) FLUXNET: A new tool to study the temporal and spatial variability of ecosystem-scale carbon dioxide, water vapor, and energy flux densities. Bull Amer Meteorol Soc 82(11):2415–2434

Belcher S, Hunt J (1993) Turbulent shear-flow over slowly moving waves. J Fluid Mech 251:109–148

Belcher S, Hunt J (1998) Turbulent flow over hills and waves. Annu Rev Fluid Mech 30:507–538

Bitsuamlak G, Stathopoulos T, Bedard C (2004) Numerical evaluation of wind flow over complex terrain: review. J Aero Eng 17:135–145
Cava D, Katul G, Scrimieri A, Poggi D, Cescatti A, Giostra U (2005) Buoyancy and the sensible heat flux budget within dense canopies. Boundary-Layer Meteorol 118:217–240
Feigenwinter C, Bernhofer C, Vogt R (2004) The influence of advection on short term CO_2 budget in and above a forest canopy. Boundary-Layer Meteorol 113:201–224
Fer I, McPhee M, Sirevaag A (2004) Conditional statistics of the Reynolds stress in the under-ice boundary layer. Geophys Res Lett 31–15:L15311
Finnigan J (1988) Air flow over complex terrain. In: Steffen WL, Denmead OT (eds) Flow and Transport in the Natural Environment: Advances and Applications, Springer-Verlag, New York: 384 pp
Finnigan J (2000) Turbulence in plant canopies. Ann Rev Fluid Mech 32:519–571
Finnigan J, Belcher S (2004) Flow over a hill covered with a plant canopy. Quart J Roy Meteorol Soc 130:1–29
Finnigan J, Brunet Y (1995) Turbulent airflow in forest on flat and hilly terrain. In Wind and Trees, vol. Wind and trees. Coutts MP, Grace J, Cambridge University Press, UK: 501 pp
Finnigan J, Raupach M, Bradley E, Aldis G (1990) A wind-tunnel study of turbulent-flow over a 2-dimensional ridge. Boundary-Layer Meteorol 50:277–317
Fokken T, Hassager C, Hipps L (2005) Editorial: surface fluxes over land in complex terrain. Theor Appl Climatol 80:79
Kader B, Yaglom A (1990) Mean fields and fluctuation moments in unstably stratified turbulent boundary layers. J Fluid Mech 212:637–662
Kaimal J, Finnigan J (1994) Atmospheric Boundary Layer Flows: Their Structure and Measurement. Oxford University Press, New York, 304 pp
Katul G, Chang W (1999) Principal length scales in second-order closure models for canopy turbulence. J Appl Meteorol 38:1631–1643
Katul G, Hsieh C, Kuhn G, Ellsworth D, Nie D (1997a) The turbulent eddy motion at the forest-atmosphere interface. J Geophys Res 102:13409–13421
Katul G, Kuhn G, Schielde J, Hsieh C (1997b) The ejection-sweep character of scalar fluxes in the unstable surface layer. Boundary-Layer Meteorol 83:1–26
Katul G, Mahrt L, Poggi D, Sanz C (2004) One and two equation models for canopy turbulence. Boundary-Layer Meteorol 113:81–109
Katul G, Porporato A, Nathan R, Siqueira M, Soons M, Poggi D, Horn H, Levin S (2005) Mechanistic analytical models for long-distance seed dispersal by wind. Amer Nat 166:367–381
Katul G, Williams C, Siqueira M, Poggi D, Porporato A, McCarthy H, Oren R (2006b) Spatial modeling of transgenic conifer pollen, Landscapes, genomics and transgenic conifers. Williams C Springer: 261 pp
Katul G, Finnigan J, Poggi D, Leuning R, Belcher S (2006a) The influence of hilly terrain on canopy-atmosphere carbon dioxide exchange. Boundary-Layer Meteorol 118:189–216
Monin A, Yaglom A (1971) Statistical fluid mechanics: mechanics of turbulence, vol. 1. The MIT Press, Cambridge: 769 pp
Nakagawa H, Nezu I (1977) Prediction of the contributions to the Reynolds stress from bursting events in open channel flows. J Fluid Mech 80:99–128
Nathan R, Katul G (2005) Foliage shedding in deciduous forests lifts up long-distance seed dispersal by wind. Proc Nat Acad Sci 102:8251–8256
Nathan R, Katul G, Horn H, Thomas S, Oren R, Avissar R, Pacala S, Levin S (2002) Mechanisms of long-distance dispersal of seeds by wind. Nature 418:409–413
Poggi D, Katul G, Albertson J (2006) Scalar dispersion within a model canopy: measurements and three-dimensional Lagrangian models. Adv Water Res 29:326–335
Poggi D, Porporato A, Ridolfi L (2002) An experimental contribution to near-wall measurements by means of a special laser Doppler anemometry technique. Exp Fluids 32:366–375
Poggi D, Katul G, Albertson J (2004a) Moment transfer and turbulent kinetic energy budgets within a dense model canopy. Boundary-Layer Meteorol 111-3:589–614
Poggi, D., Porporato A, Ridolfi L, Katul G, Albertson J (2004b) The effect of vegetation density on canopy sublayer turbulence. Boundary-Layer Meteorol 111-3:565–587
Raupach M (1981) Conditional statistics of the Reynolds stress in rough-wall and smooth-wall turbulent boundary layers. J Fluid Mech 108:363—382
Raupach M, Shaw R (1982) Averaging procedures for flow within vegetation canopies. Boundary-Layer Meteorol 22-1:79–90

Ross A, Vosper S (2005) Neutral turbulent flow over forested hills. Quart J Roy Meteorol Soc 131:1841–1862
Shaw R, Tavangar J, Ward D (1983) Structure of the Reynolds stress in a canopy layer. J Clim Appl Meteorol 22:1922á1-1931
Soons M, Heil G, Nathan R, Katul G (2004) Determinants of long-distance dispersal by wind in grasslands. Ecology 85:3056–3068
Staebler R, Fitzjarrald D (2004) Observing subcanopy CO_2 advection. Agr Forest Meteorol 122:139–156
Tennekes H, Lumley J (1972) A first course in turbulence, vol. I. MIT Press, Cambridge, MA: 300 pp
Wilson N, Shaw R (1977) A higher order closure model for canopy flow. J Appl Meteorol 16:1198–1205